

Scatterometer wind fields: A new release over the decade 1991–2001

Abderrahim Bentamy, Yves Quilfen, and Pierre Flament

Abstract. The global surface wind fields calculated from scatterometer observations have been updated to cover the decade 1991–2001. This involves an enhancement of the remotely sensed wind retrievals, quality control, and objective method. This paper presents the improvements with respect to the first release and provides the main characteristics of the surface parameter fields. The accuracy of the resulting weekly and monthly surface wind fields is studied through comparisons with buoy and numerical model averaged wind estimates.

Résumé. Les champs globaux de vent de surface calculés à partir des observations des diffusiomètres ont été mis à jour pour couvrir la période 1991–2001. Ceci implique une amélioration de la procédure de restitution des vents diffusiométriques, du contrôle qualité, et de la méthode objective. Cet article présente les améliorations en ce qui concerne la première version, et fournit les caractéristiques principales des vents de surface. La qualité des champs hebdomadaires et mensuels de vent avec étudiée à travers des comparaisons avec les moyennes des vents mesurés par des bouées ou estimés par un modèle numérique.

Introduction

Surface wind fields are important in a wide variety of atmospheric and oceanic processes. They are required, for instance, to drive ocean models and to validate coupled ocean–atmosphere global models. Because of the extent of the oceans, few wind data are available from buoys, ships, and other in situ instruments. Satellite microwave measurements are considered the most reliable means for global estimation of oceanic wind vectors. They are routinely used for several oceanographic and atmospheric purposes. For instance, since 1996 the European Centre for Medium-Range Weather Forecasts (ECMWF) has assimilated ERS-2 scatterometer wind data. Furthermore, several authors have shown the positive impact of the scatterometer wind observations on numerical weather prediction (NWP) (see, for instance, Andrews and Bell, 1998; Atlas, 1997; and Stoffelen and Anderson, 1997). Surface winds derived from NWP, however, are related to numerical model constraints, are not accurate enough for various climate and ocean applications, and are characterized by particularly poor spatial resolution (Barnier et al., 1994; Millif et al., 1996). For several scientific studies, data sets are requested that are only related to measurements and their characteristics (Grima et al., 1999). Such data sets can also in turn be used to evaluate the accuracy of NWP wind estimates.

Gridded surface wind parameters, including wind vector, stress, curl, and divergence, have been computed since August 1991 from three satellite microwave scatterometers: the Active Microwave Instrument (AMI) on board the European Remote Sensing Satellites ERS-1 and ERS-2 (ERS-1/2), and the National Aeronautic and Space Administration (NASA) scatterometer (NSCAT) on board the Advanced Earth Observing Satellite (ADEOS1). These instruments measure backscatter from the sea surface to provide global, near-surface

wind speeds and directions with a spatial resolution of 50 km over a swath of 500 km for the ERS-1/2 and over two 600 km swaths for the NSCAT.

These gridded winds have been used extensively in global wind studies (Bentamy et al., 1998) and in ocean model forcing (Grima et al., 1999; Quilfen et al., 2000). Forcing experiments with gridded scatterometer wind fields indicated that the correlation between the thermocline from the ERS-1 simulation and from buoy measurements is statistically significant at a level greater than 0.70 in the tropical regions.

Some problems remain, however. Gridded ERS wind speeds are biased low compared with buoy estimates, especially in the eastern tropical Pacific. Furthermore, for wind fields estimated from the ERS-1, some wind patterns are mainly due to the sampling scheme, especially in regions of high wind variability (Ebutchi and Wada, 2001). Therefore, additional studies were performed to improve the quality of gridded scatterometer wind fields.

In this paper we present a new release of weekly and monthly gridded wind fields derived from scatterometer wind observations. A previous analysis of surface wind fields (Bentamy et al., 1998) was performed only with ERS-1 scatterometer data spanning the period 1991–1996. The present work deals with the improvement of the procedures used to retrieve surface winds and estimate global weekly and monthly wind fields. Winds derived from ERS-1, ERS-2, and NSCAT scatterometer data from August 1991 through January 2001 are now included.

Received 9 October 2001. Accepted 25 February 2002.

A. Bentamy,¹ Y. Quilfen, and P. Flament. Institut Français pour la Recherche et l'Exploitation de la MER (IFREMER), BP 70, 29280 Plouzané, France.

¹Corresponding author (e-mail: Abderrahim.Bentamy@ifremer.fr).

The first section of the paper provides a description of data, the objective method used, and the sampling errors. The following two sections deal with estimating the accuracy of scatterometer wind fields, including a comparison with buoy and ECMWF winds, and the final section discusses some surface wind features characteristic of the resulting gridded fields.

Data and methods

Wind observations

The ERS-1 scatterometer operated from August 1991 to May 1996, and the ERS-2 scatterometer from March 1996 to January 2001. Both provided near-surface wind vectors over the global ocean, with a spatial resolution of 50×50 km and a swath width of 500 km. The NSCAT operated from September 1996 to June 1997, with two 600 km swaths (NSCAT simultaneously scans two 600 km bands of the Earth) separated by a gap of 400 km. In this study, only NSCAT data at 50 km resolution were used. There are about 14.3 ERS-1/2 and NSCAT orbits per day, and thus they cover the global ocean within 3 and 2 days, respectively. The ERS scatterometer makes about 79 500 wind observations per day, and the NSCAT about 190 000 observations per day.

The accuracy of wind speed and direction retrieved from the ERS and NSCAT was determined by comparing with buoy hourly estimates. Three buoy networks were used (**Figure 1**): the National Data Buoy Center (NDBC) buoys off the Atlantic, Pacific, and Gulf of Mexico coasts of the United States; the tropical atmosphere ocean (TAO) buoys located in the tropical Pacific Ocean and maintained by Pacific Marine Environmental Laboratory (PMEL); and the ODAS buoys located off the European coasts and maintained by the United Kingdom Meteorological Office and Meteo-France.

The NDBC buoys have a propeller-vane anemometer at a height of 5 m which records hourly an 8 min average wind speed and a single direction with an accuracy of 1 m/s and 10° (Gilhousen, 1987). The TAO buoys measure winds at a height of 3.8 m using a propeller-vane anemometer. Wind speed and

direction are both sampled at 2 Hz and vector-averaged for 1 h (Hayes et al., 1991). The ODAS buoys have a cup anemometer and wind vane at a height of 4 m that record hourly a 10 min average wind speed and direction (only ODAS measurements for the NSCAT period are used here). The calculation of buoy wind speeds at a height of 10 m in neutral conditions is performed using the LKB model (Liu et al., 1979). Hourly buoy wind speed and direction are used in the scatterometer–buoy comparisons.

Estimates of the surface wind fields over the global ocean are routinely generated in the ECMWF. Several studies used the ECMWF wind analysis for assimilation, forcing, and comparison purposes and indicate that the ECMWF wind products represent the global wind patterns as best we know them. The ECMWF forecast-analysis system assimilates various measurements from buoys, ships, aircraft, cloud-tracked-drift, radiosondes, and satellites. The ECMWF operational wind analysis is performed four times daily at spatial resolution T213 (about 100 km horizontal resolution; for more details see ECMWF, 1995). The ECMWF wind speed at a height of 10 m is computed from zonal (u) and meridional (v) wind components, i.e., $W_{ECMWF} = (u^2 + v^2)^{1/2}$, at each synoptic time (00:00, 06:00, 12:00, 18:00).

Accuracy of the scatterometer wind observations

By collocating in space and time satellite and buoy measurements, Graber et al. (1996) indicate that the ERS-1 scatterometer wind speeds are biased low compared with buoy winds. The biases derived from the ERS-1 versus the NDBC and from the ERS-1 versus the TAO comparisons are 0.30 and 1 m/s, respectively, with root mean squared (RMS) errors of 1.13 and 1.38 m/s, respectively. The RMS error direction is 24° for both buoy networks. Using a similar collocation procedure, Graber et al. showed that the difference between the NDBC and the NSCAT wind speeds had mean and RMS values of 0.14 and 1.22 m/s, respectively. The RMS error in direction is about 24° . For the NSCAT–TAO comparisons (Caruso et al., 1999), the wind speed bias is very low and the RMS difference is about 1.55 m/s. The RMS error in direction is about 20° . The ERS-2

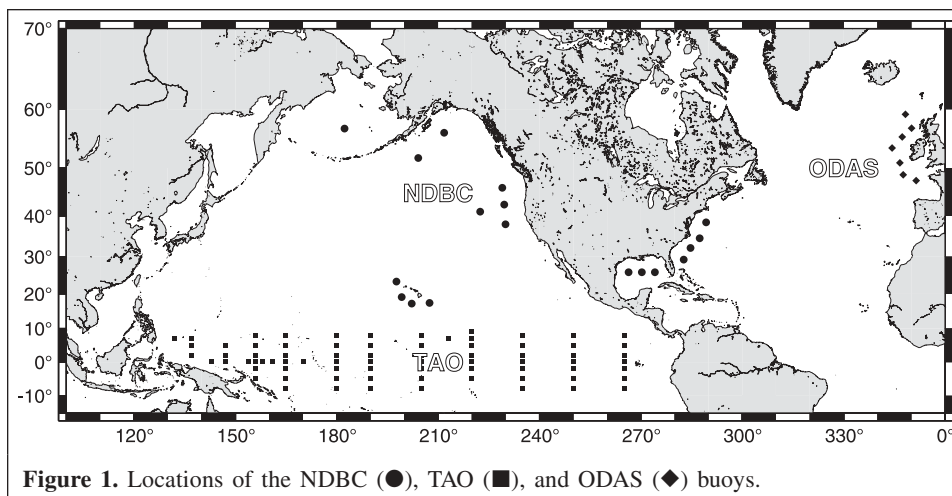


Figure 1. Locations of the NDBC (●), TAO (■), and ODAS (◆) buoys.

results are similar to those for ERS-1, however, the bias for ERS-2 is higher than that for ERS-1 (Quilfen et al. 1999). **Figure 2** shows scatterplots comparing the ERS-2 and NSCAT wind speeds with buoy winds at 10 m for the NDBC, TAO, and ODAS buoys. All validated buoy and scatterometer wind data were collocated within spatial and temporal windows of 1 h and 50 km, respectively, during the NSCAT period October 1996 – June 1997. Most statistical parameters, provided within each figure, are similar to those cited earlier. The bias on ERS-2 wind speed, however, is significant and requires correction.

To enhance the quality of the ERS-1/2 scatterometer wind speeds, they were collocated against the NDBC buoys. The TAO and ODAS measurements are used for validation purposes. All valid measurements within 1 h and 50 km of the NDBC buoy measurements were selected during the period March 1992 – November 1998 and used to derive a new version of the ERS C-band model used to retrieve scatterometer wind speed from measured backscatter coefficients. The method developed in Bentamy et al. (1994) is used to achieve such an ERS scatterometer calibration. The accuracy of the new C-band model is determined through comparisons between buoy and retrieved scatterometer wind speeds. For instance, the biases for the ERS-2 wind speed, calculated with respect to the TAO and ODAS winds, are reduced to 0.60 and 0.16 m/s, respectively. The corresponding RMS values are 1.52 and

1.55 m/s. Hence, the ERS-1/2 gridded wind fields are calculated from the new corrected wind speeds and from the standard wind directions (Maroni, 1995).

Objective method

The details of the calculations of the gridded wind field from scatterometer observations are provided by Bentamy et al. (1996). The observations are objectively analyzed using the kriging method. At each grid point the weekly or monthly wind vectors are estimated by interpolating scatterometer wind speeds, zonal components, and meridional components. The weekly and monthly wind direction is derived from averaged wind components. For each variable, the estimator at grid point X_0 using N observations at point X_i is

$$\hat{U} = \sum_{i=1}^N \lambda_i V(X_i) \quad \sum_{i=1}^N \lambda_i = 1 \quad (1)$$

where \hat{U} is the wind speed, zonal component, or meridional component; $V(X_i)$ are the corresponding scatterometer observations at the spatial and temporal coordinates X_i ; and the weights λ_i are determined as the minimum of the linear system, called the kriging system:

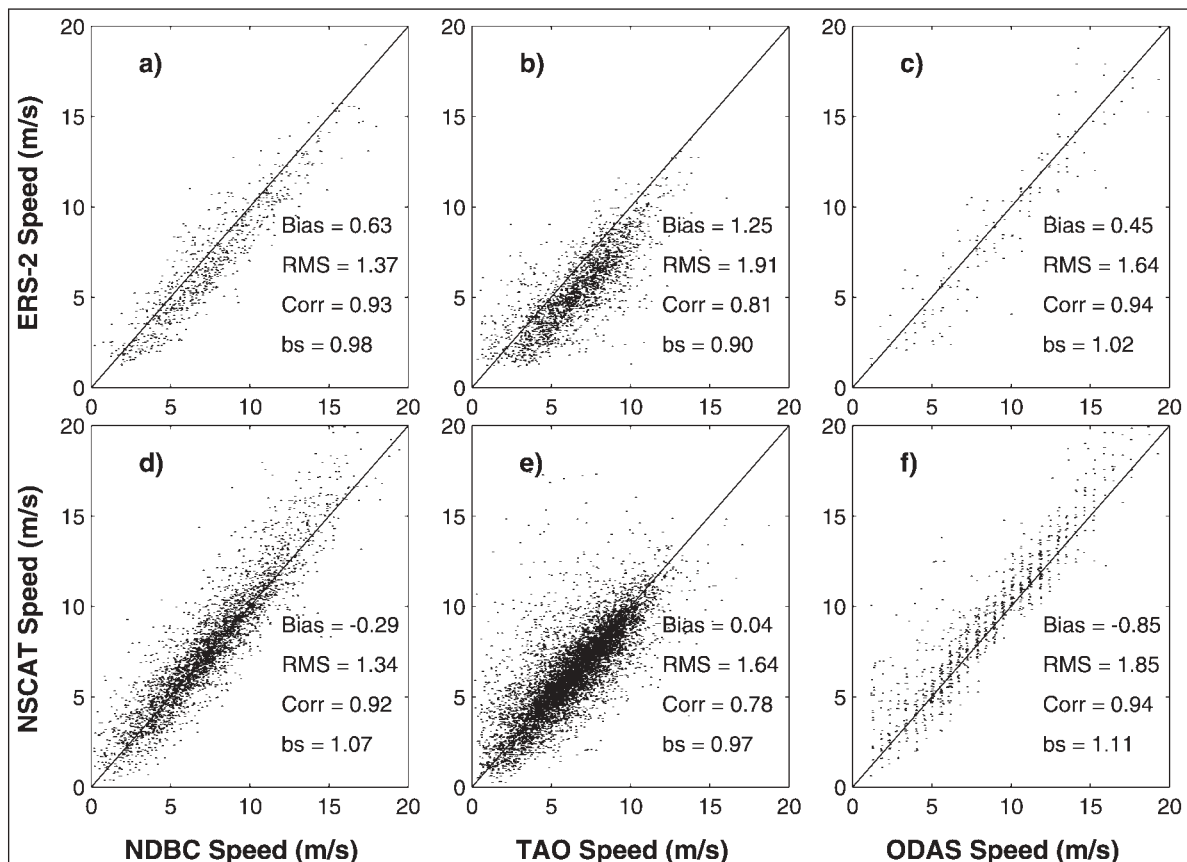


Figure 2. Scatterplots of collocated wind speeds derived from buoy measurements (NDBC, TAO, and ODAS) and from scatterometer observations (ERS-2 and NSCAT). bs, slope of the symmetrical regression line; Corr, correlation coefficient; RMS, root mean squared.

$$\begin{aligned}
 & -\sum_{i=1}^N \lambda_i \Gamma(i, j) + \Gamma(j, 0) - \tau + \lambda_j \sigma^2 = 0 \\
 & \sum_{i=1}^N \lambda_i = 1 \quad j = 1, N
 \end{aligned} \tag{2}$$

where τ and σ^2 are the Lagrangian multiplier and variance of the wind variable, respectively (for more details, see Bentamy et al., 1996); and Γ is the structure function representing the spatial and temporal behavior of the variable estimated. Γ is estimated directly from the ERS-1 scatterometer wind speed, zonal component, and meridional component observations. It should be noted that there is no change in the variogram analytic form or in its parameters with respect to the previous release (Bentamy et al., 1996). In Equation (3), $\Gamma(i, j)$ indicates the variogram value i.e., the dissimilarity between the data points X_i and X_j . $\Gamma(j, 0)$ indicates the dissimilarity between X_j and X_0 .

The kriging method provides an expression for the error E of the estimated wind variable at each grid point:

$$E[(\hat{U} - U)^2] = \Gamma(0,0) + \tau + \sum_{i=1}^N \lambda_i \Gamma(i,0) \tag{3}$$

where U is the wind variable.

In practice, the procedure is outlined as follows:

- (1) The scatterometer wind products, including backscatter measurements and retrieved wind vectors, are extracted from the Centre ERS d'Archivage et de Traitement (CERSAT) data base. They have been generated as the off-line ERS-1/2 (Maroni, 1995) and NSCAT (Jet Propulsion Laboratory, 1998) scatterometer wind products. Only validated data, according to standard quality controls, are used.
- (2) At each ERS-1/2 scatterometer cell (50 km), a new wind speed is estimated from the three backscatter coefficients using the new C-band model function. The direction selected by the operational algorithm is chosen. For low wind speeds (less than 3 m/s), however, the ECMWF wind direction is used to select the scatterometer wind direction among the different aliases.
- (3) At each grid point ($1 \times 1^\circ$), a subset (neighborhood) of the surrounding measured data is defined. It is a sensitive step because of the irregular spatial and temporal sampling and the variable density of the observations. A local neighborhood is determined as successive circles centered on a grid point (CERSAT, 1998). The radius of these circles corresponds to the variogram parameters. In the first release of the gridded winds, the number of the scatterometer wind observations used for each grid point was limited to 20, resulting in noisier estimates (Ebutchi and Wada, 2001). In the present study, there is no limit

on this number, which may reach 1200, especially for monthly and NSCAT fields. These observations are then sorted by time, and for each hour the closest scatterometer observations (V in Equation (1)) to the grid point are selected. The selected scatterometer "instantaneous" observations are then used to estimate the wind vector using the kriging method. For instance, in an equatorial region, an average of 22 ERS and 38 NSCAT observations are selected over 1 week to estimate the weekly averaged wind vector at a grid point. An example of gridded wind fields (wind speed and wind direction), derived from ERS-2 and NSCAT wind observations, is shown in **Figure 3**.

Sampling error

To examine the features of the resulting wind fields and especially the impact of the sampling scheme on the calculations, we have simulated scatterometer wind observations from a known wind field and directly compared averages of the sampled values with "true" mean quantities obtained from the ECMWF surface analyses. The latter are used as the true wind field. As indicated in the section Wind observations, the temporal and spatial resolution of the ECMWF wind analysis is 6 h and $1.125 \times 1.125^\circ$. Therefore, to define the simulated scatterometer data, the ECMWF analyses are interpolated in space and time to the scatterometer (ERS-2, NSCAT) measurement cells and times for wind speed and wind components. The error due to the interpolation scheme is investigated through a comparison between the ECMWF and simulated scatterometer observations collocated within space and time windows of 50 km and 3 h. For instance, the zonal component RMS errors, due to the interpolation method used to estimate ECMWF on ERS-2 scatterometer cells, calculated in tropical and high-latitude oceans and during 1 week in January 1997, are about 0.60 and 0.95 m/s, respectively. This RMS is referred to as the simulated scatterometer data error.

The gridded wind fields calculated from scatterometer wind observations (ERS-1/2 and NSCAT) are referred to as scatterometer wind fields, and wind fields estimated from the ECMWF wind analysis interpolated (in space and time) to scatterometer cells are referred to as simulated scatterometer wind fields. The averaged wind fields derived from a standard ECMWF 6 h wind analysis with a grid point of $1 \times 1^\circ$ are called true wind fields. Their calculation is performed using a simple arithmetic averaging process. Even though this study is mainly concerned with weekly and monthly wind field characteristics, several averaging times are investigated. The time-averaged simulated scatterometer and true wind fields are computed through the objective method (see the previous section) and the arithmetic averaging process, respectively. **Figure 4** shows the RMS error of the difference between gridded zonal wind components, derived from true and simulated scatterometer data, as a function of averaging time varying between 1 and 10 days. The calculations of both wind fields are performed from data collected between 1 and 10 June 1997. **Figures 4a**

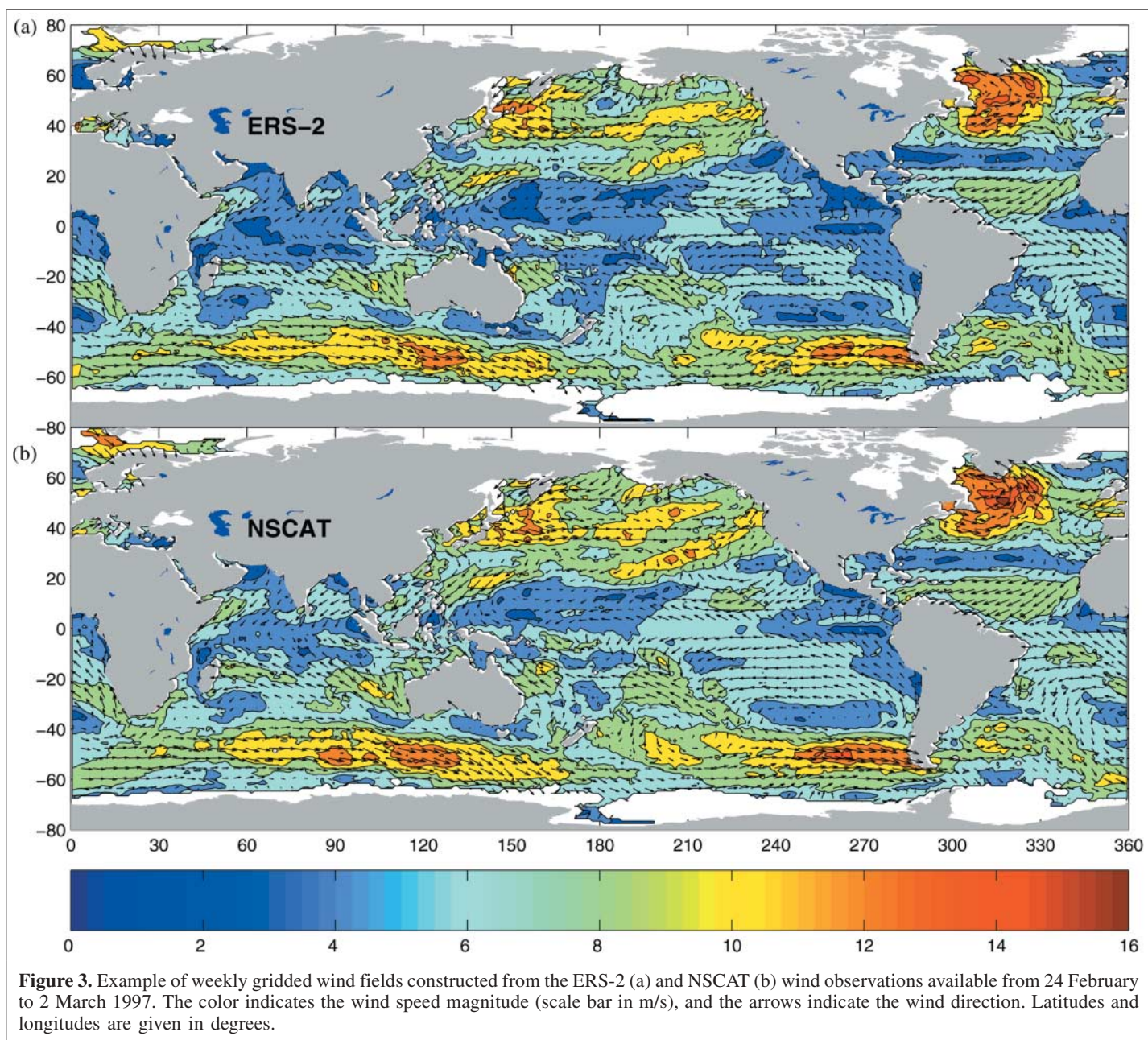


Figure 3. Example of weekly gridded wind fields constructed from the ERS-2 (a) and NSCAT (b) wind observations available from 24 February to 2 March 1997. The color indicates the wind speed magnitude (scale bar in m/s), and the arrows indicate the wind direction. Latitudes and longitudes are given in degrees.

and 4b show the results obtained in the tropical oceans (5°N–5°S) and in the Southern Ocean (45°S–55°S). In the first area, the scatterometer sampling length is poor and the wind variability is low. The second region is well known for its high wind variability compensated by a larger number of scatterometer observations falling into each grid point of $1 \times 1^\circ$. In tropical areas, and with respect to simulated scatterometer data errors (see earlier), an accurate gridded wind field is expected for averaging time longer than 6 days for ERS-2 and 2 days for NSCAT. At high latitudes, an accurate wind field derived from ERS-2 is obtained for 9 days, whereas for NSCAT a 2 day averaging time is satisfactory. Therefore, a sampling error, varying between 0.6 and 1.2 m/s for ERS-1/2 and between 0.4 and 0.6 m/s for NSCAT, is expected for

weekly wind fields. This error involves the ECMWF analysis interpolation on scatterometer swaths.

The analysis of the scatterplot comparison between true and simulated weekly wind fields does not exhibit any systematic errors in the wind estimates (not shown). In general, the difference between the two fields varies between -1.5 and 1.5 m/s (in terms of zonal component). Some high values are found, however, and correspond to regions where wind variability is high and (or) the scatterometer sampling number is low (Bentamy et al., 1998). For instance, difference values exceeding 2 m/s are observed in the extratropical northern latitudes. In such regions, the standard deviation of the ECMWF zonal wind component is six times higher than that in the region where the difference between true and simulated scatterometer gridded wind fields is low. It is not surprising that

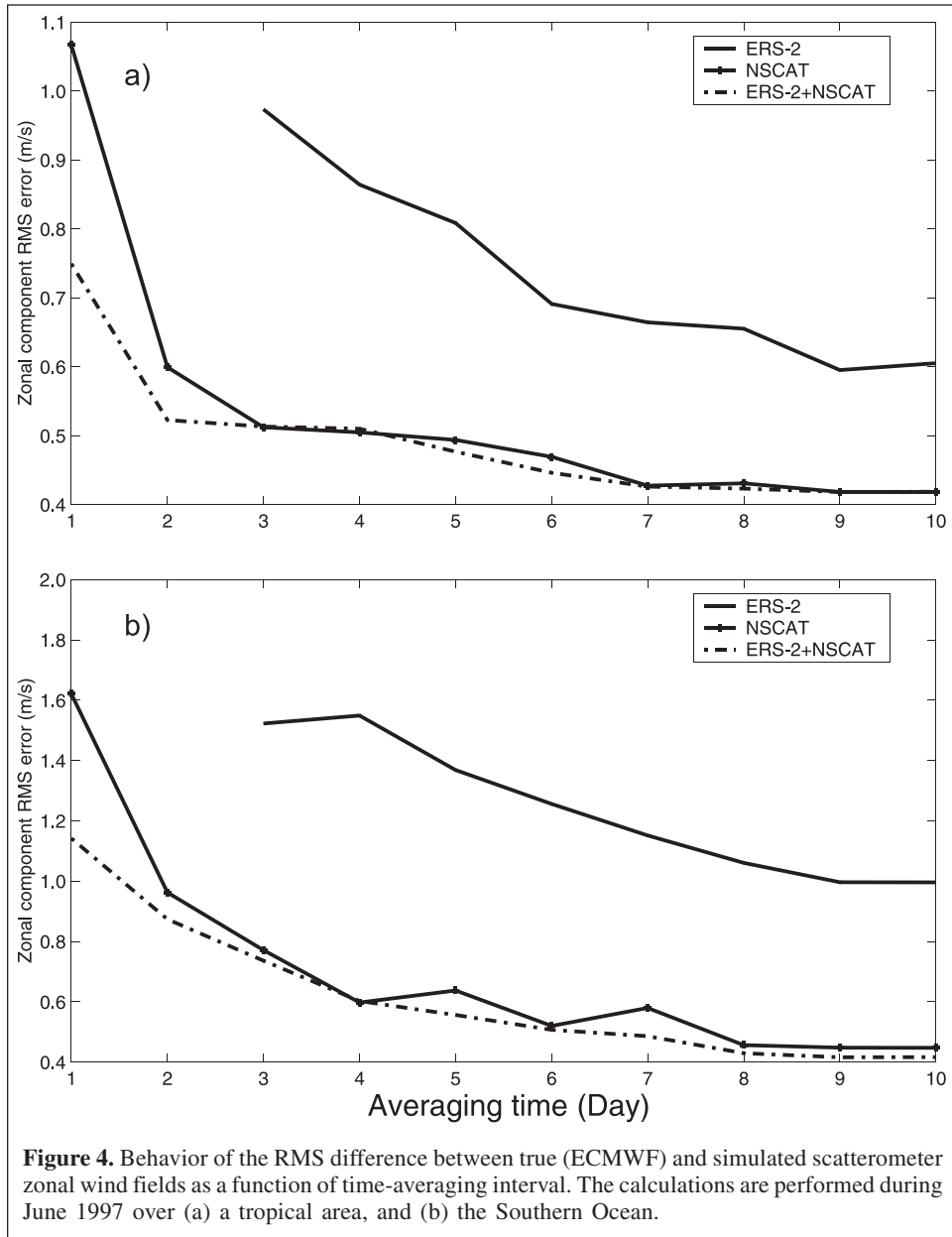


Figure 4. Behavior of the RMS difference between true (ECMWF) and simulated scatterometer zonal wind fields as a function of time-averaging interval. The calculations are performed during June 1997 over (a) a tropical area, and (b) the Southern Ocean.

the NSCAT sampling scheme is a significant remedy to such problems compared to gridded wind fields estimated from the ERS-1/2. For instance, let us consider the resulting wind field features at the equator and latitude 35°S. **Figures 5 and 6** show the behavior of weekly zonal components derived from simulated ERS-2 and NSCAT data and from ECMWF wind analysis, respectively, along these latitudes, as a function of longitude. The figures show that the agreement between the three estimates is good. The correlation values, estimated at the equator, between simulated and true variables are about 98% for the ERS-2 and 99% for the NSCAT. In the Southern Ocean, the correlation drops to 97% for the ERS-2, while for NSCAT it remains greater than 98%. The main discrepancies are observed at 35°S, between longitudes 245° and 250° and 335° and 345° (**Figure 6c**). In these bands the number of simulated scatterometer data within each grid point is the maximum

(between 4 and 7 for the ERS-2 and between 10 and 15 for the NSCAT). These differences are mainly due to the ECMWF wind variation over the week. For instance, between longitudes 335° and 345°, the standard deviation of 6 h ECMWF winds is higher than 8 m/s and its mean value is about 5 m/s. It is obvious that such a wind event cannot be retrieved easily with a limited number of satellite observations falling into each grid point of the area. **Figures 5 and 6** show that the ERS-2 zonal component does not exhibit any systematic 500–1000 km wavelength oscillations (Large, 1998).

Similar investigations were performed for monthly gridded wind fields. As expected, the differences are reduced drastically with respect to weekly wind field estimates. The highest values of the difference between the true and simulated zonal component do not exceed 2.20 m/s. The percentage of grid points, with respect to total grid point number, where the

difference between the ECMWF and simulated scatterometer zonal components exceeds 1.20 m/s, accounts for 4% for ERS-2 and 1% for NSCAT simulations. Most of these high difference values are found at high latitudes.

Table 1 summarizes the main statistical parameters characterizing scatterometer sampling impact on the gridded wind field calculations. These parameters are estimated for June 1997 over the global oceans: σ_D is the standard deviation of the wind field difference; and ϵ is the ratio σ_D/σ_E , where σ_E is the standard deviation of the ECMWF weekly wind field. **Table 1** indicates that the gridded wind fields estimated from

simulated data are unbiased according to the ECMWF mean wind field. The highest value of the standard deviation σ_D , characterizing the deviation of weekly simulated wind fields from the ECMWF mean wind field, does not exceed 1 m/s. We notice, however, that 19% of the standard deviation values for ERS cases and 10% for NSCAT cases are mainly due to the scatterometer sampling. Calculation of the zonal mean of ϵ indicates that its minimum values are obtained in the tropical oceans (20°N–20°S): 15% for the ERS-2 and 8.5% for the NSCAT.

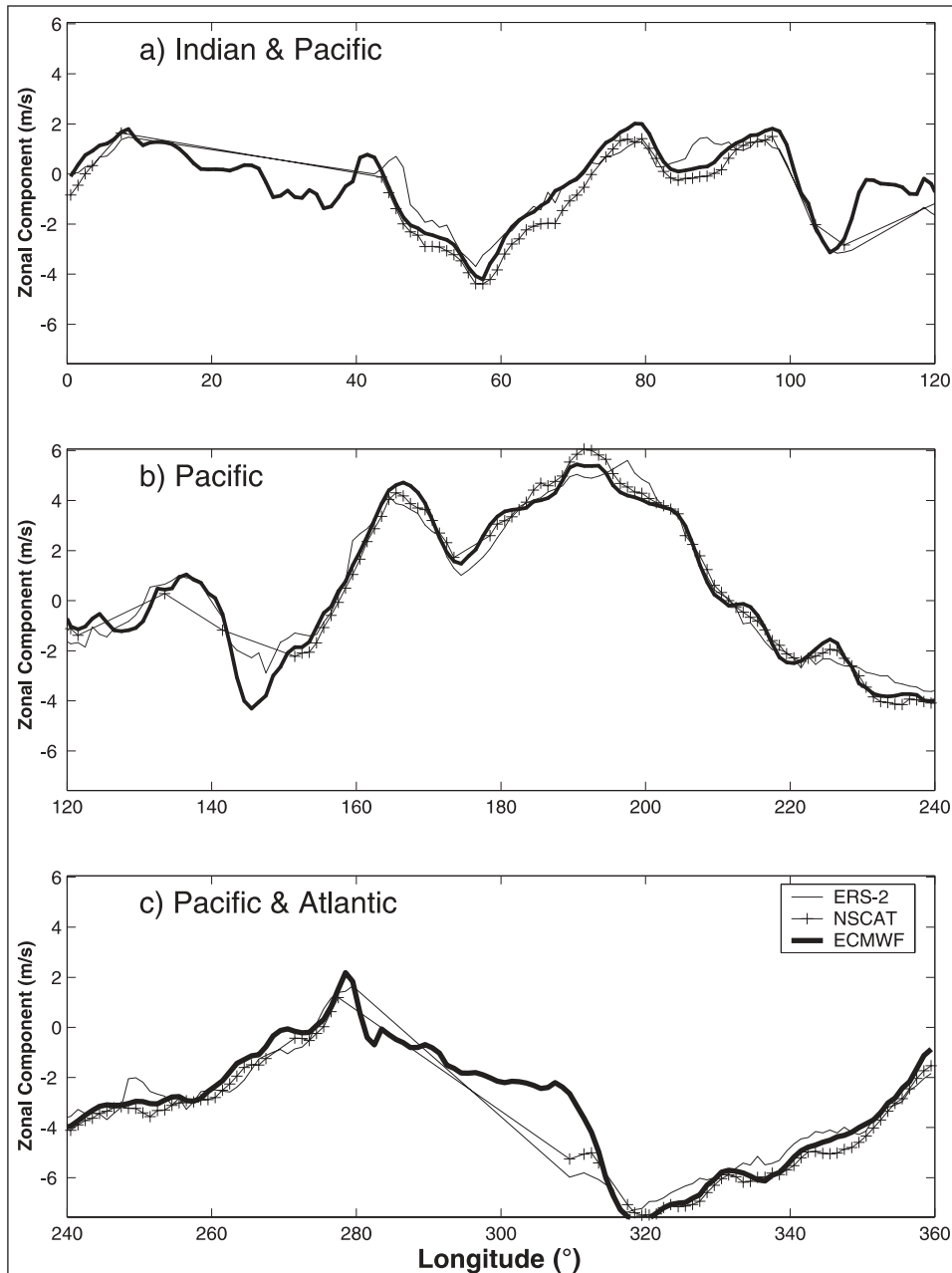


Figure 5. Evolution of weekly zonal component estimated from the simulated ERS-2, from the NSCAT, and from the ECMWF 6 h analysis wind data as a function of longitude. Calculations are performed for June 1997 at the equator.

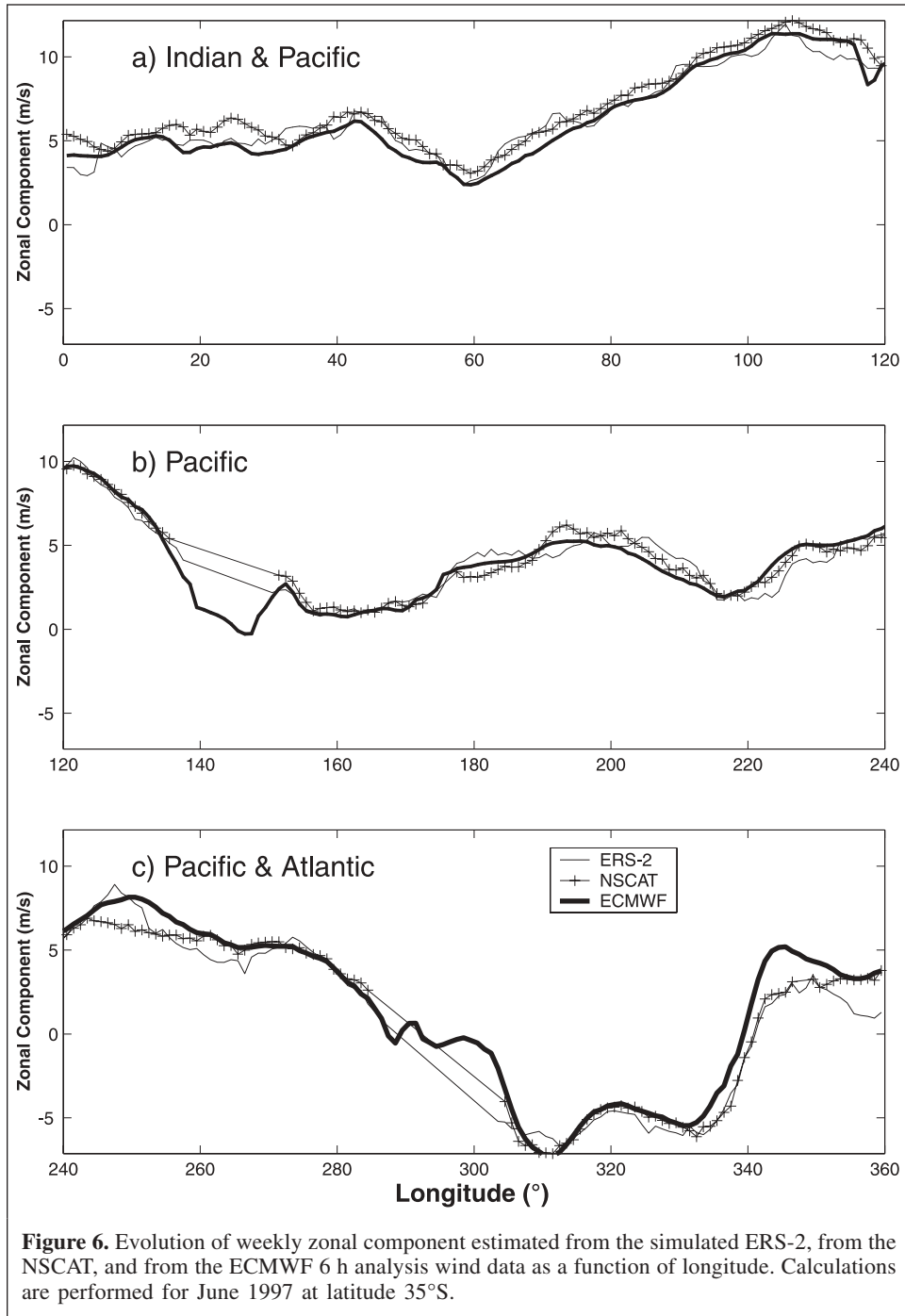


Figure 6. Evolution of weekly zonal component estimated from the simulated ERS-2, from the NSCAT, and from the ECMWF 6 h analysis wind data as a function of longitude. Calculations are performed for June 1997 at latitude 35°S.

For monthly wind fields, we observe that the value of ϵ reduces to 13% and 8% for the ERS-2 and NSCAT, respectively. The calculations of the zonal mean of ϵ indicates that its values are quite similar over the global oceans.

Scatterometer- and buoy-averaged wind comparisons

For each week and each month, the mean values of buoy wind speed and zonal and meridional components are computed arithmetically. Weekly and monthly means are

computed for all ERS-1, ERS-2, and NSCAT periods when at least 3.5 day and 15 day buoy measurements are collected, respectively. For each averaging period, the closest scatterometer grid point ($1 \times 1^\circ$) to each buoy location is selected. Therefore, collocated data sets between scatterometer gridded wind fields (averaging objective method) and buoy-averaged winds are performed for the NDBC, TAO, and ODAS buoy networks. It is important to point out that a part of the NDBC hourly wind observations was used to calibrate the ERS scatterometer empirical model. Therefore, the comparisons between scatterometer- and NDBC-averaged wind estimates

Table 1. Statistical parameters of the scatterometer wind speed sampling error.

	Mean (m/s)	σ_D (m/s)	ϵ
Weekly wind fields			
ECMWF vs. ERS-2	0.09	0.96	0.19
ECMWF vs. NSCAT	0.04	0.50	0.10
Monthly wind fields			
ECMWF vs. ERS-2	0.04	0.59	0.13
ECMWF vs. NSCAT	0.04	0.38	0.08

should be considered as an examination of the quality of the resulting gridded wind field. However, all the TAO and ODAS winds were not used for the ERS scatterometer calibration.

The comparisons between buoy- and scatterometer-averaged winds use the following standard statistical data analysis:

- (1) The wind speed, zonal component, and meridional component are assumed to be random variables, which could be characterized by their moments. For this purpose, the two conventional moments of each variable are estimated.
- (2) Some statistical parameters are estimated to assess the comparisons between satellite gridded wind fields and buoy-averaged winds. Let x and y denote the buoy and scatterometer wind estimates, respectively. Through this study, the following parameters are calculated: bias = $\langle x - y \rangle$; root mean square (RMS)

$$RMS = \sqrt{\langle (x - y)^2 \rangle}; \tag{4}$$

slope of symmetrical regression (bs)

$$bs = \sqrt{\frac{\langle (y - \bar{y})^2 \rangle}{\langle (x - \bar{x})^2 \rangle}}; \tag{5}$$

and correlation coefficient (ρ)

$$\rho = \frac{\langle (x - \bar{x})(y - \bar{y}) \rangle}{\sqrt{\left(\langle (x - \bar{x})^2 \rangle \langle (y - \bar{y})^2 \rangle \right)}} \tag{6}$$

The parameter ϵ is the difference between y and the linear regression model $y = bx + a + \epsilon$, where b is the slope of the regression line and a is the intercept on the y axis. For wind direction, the mean angle difference and the standard deviation (SD) of angular difference are calculated as defined in Graber et al. (1996).

Global comparisons

Table 2, 3, and 4 provide the statistics from the wind speed comparisons. The wind speed correlation coefficients are significant and range from 0.85 to 0.89. The RMS values of the buoy–satellite differences do not exceed 1.16 m/s over the NDBC and TAO networks, but are higher for the ODAS comparisons: 1.48 m/s for NSCAT and 1.66 m/s for ERS-2. This is mainly as a result of a smaller number of comparison data points and high wind variability in the ODAS area (**Figure 1**). Furthermore, the statistics calculated by several meteorological centers (ECMWF, Centre de Meteorologie Spatiale of Meteo France (CMM), U.K. Meteorological Office) indicate that the ODAS buoy wind speed tends to be underestimated according to meteorological wind analysis (see the site maintained by P. Blouch at <ftp://ftp.shom.fr/meteo/qc-stats>). The statistical parameters are also calculated in bins of 5 m/s of the buoy wind speed. Their values show a small dependence on the NDBC and TAO wind speed. The bias is slightly positive for the ERS and negative for the NSCAT in the whole range of wind speeds. The analysis carried out on collocated data (**Figure 7**) shows that the slopes calculated over each buoy network and against buoy wind estimates are similar, regardless of the three scatterometer winds used for comparison. For the NDBC (**Table 2**), buoys and scatterometers correlate closely, as expressed by slopes (b and bs) of about 1 and intercepts of about zero. For the TAO data in the tropical Pacific Ocean, slopes are about 0.90, suggesting an overestimation of low wind speed and an underestimation of high wind speed by scatterometer wind fields compared with the TAO winds. In the North Atlantic area, the slopes are close to 1, whereas the intercepts are about 0.50, indicating that the scatterometer wind fields are consistently high compared with the ODAS weekly averaged wind speeds. The calculation of statistical parameters according to the ODAS buoy wind speed ranges shows that their values are made variable by the outlying points at low and high wind speeds.

No systematic wind direction bias is found, and the overall bias and standard deviation in terms of the mean angular difference are less than 8° and 38° , respectively. These results are consistent with the calibration–validation of scatterometers against buoys (Graber et al., 1996; 1997; Caruso et al., 1999). For instance, in the Pacific tropical area, where the wind direction is quite steady, the standard deviation calculated for buoy wind speeds higher than 5 m/s does not exceed 17° .

Time series

The agreement between averaged wind fields from scatterometers and buoys can be studied using time series. **Figure 8** shows examples of weekly averaged time series of wind speed at three buoy locations in the NDBC and TAO arrays. The time series indicate that the matchups are strongly correlated and their geographical features compare well. The lowest correlation values (less than 0.91) are found in the TAO array. For the TAO array at 2°N and 95°W (**Figure 8c**), the

Table 2. Comparison of averaged weekly wind speed and direction estimated from the NDBC buoy measurements and from the ERS-1, ERS-2, and NSCAT scatterometer observations.

Buoy wind speed range (m/s)	Length	Wind speed			Wind direction	
		Bias (m/s)	RMS (m/s)	ρ	Bias ($^{\circ}$)	SD ($^{\circ}$)
NDBC vs. ERS-1						
0–24	3281	0.02	1.16	0.86	3	35
0–5	320	–0.14	1.03	0.74	5	47
5–10	2603	0.05	1.16	0.83	3	34
>10	358	–0.00	1.31	0.76	3	30
NDBC vs. ERS-2						
0–24	1921	0.35	1.15	0.86	6	33
0–5	142	0.06	0.82	0.75	0	47
5–10	1581	0.37	1.16	0.83	6	33
>10	198	0.40	1.26	0.77	6	25
NDBC vs. NSCAT						
0–24	522	–0.37	1.02	0.88	8	25
0–5	28	–0.54	0.94	0.76	3	29
5–10	444	–0.37	1.01	0.85	8	26
>10	50	–0.32	1.15	0.79	7	15

Note: Bias, root mean squared (RMS), correlation coefficient (ρ), and standard deviation characterizing the difference between buoy and scatterometer averaged wind speeds and directions are provided.

Table 3. Comparison of averaged weekly wind speed and direction estimated from the TAO buoy measurements and from the ERS-1, ERS-2, and NSCAT scatterometer observations.

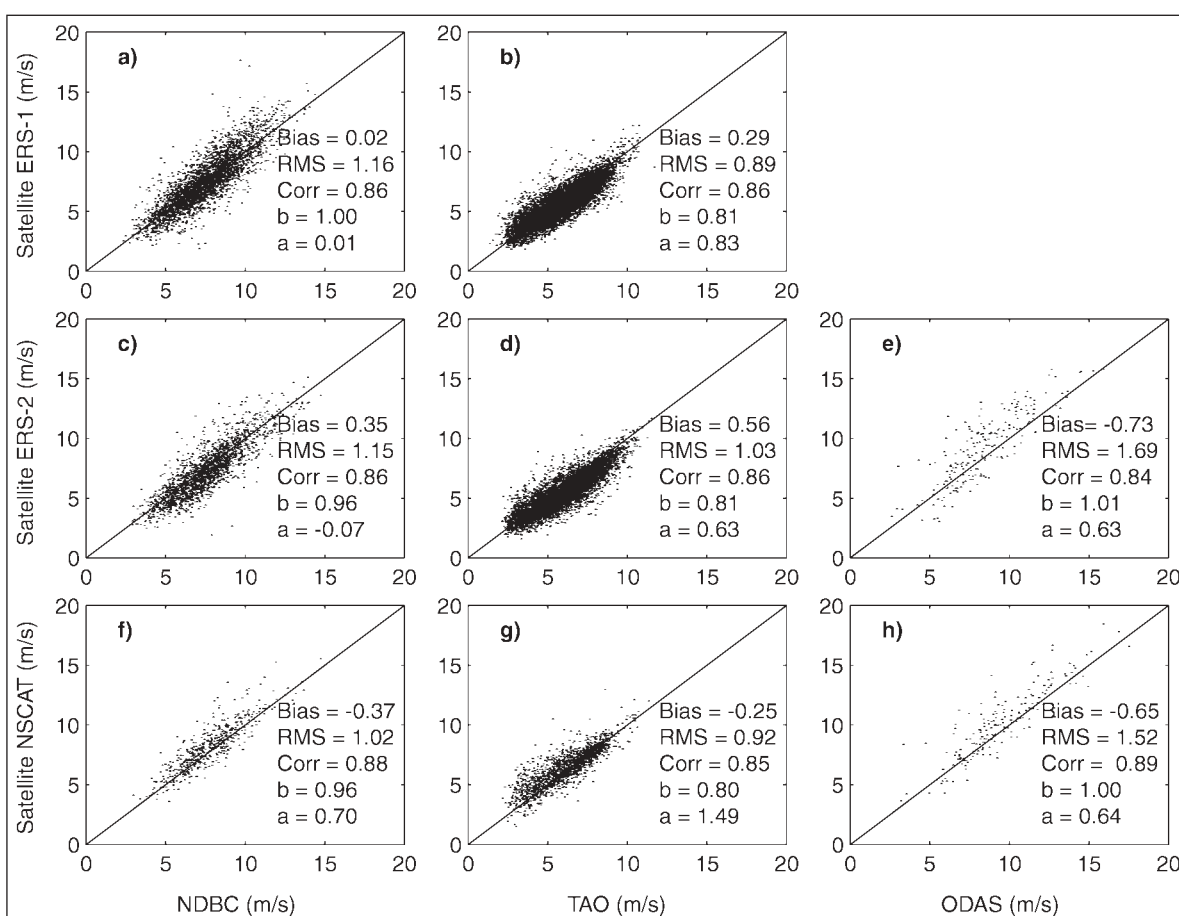
Buoy wind speed range (m/s)	Length	Wind speed			Wind direction	
		Bias (m/s)	RMS (m/s)	ρ	Bias ($^{\circ}$)	SD ($^{\circ}$)
TAO vs. ERS-1						
0–24	10 047	0.29	0.89	0.86	3	31
0–5	3 262	–0.14	0.85	0.76	1	51
5–10	6 693	0.47	0.91	0.84	5	17
>10	92	0.24	0.92	0.70	8	9
TAO vs. ERS-2						
0–24	6 737	0.56	1.03	0.86	3	27
0–5	1 925	0.06	0.84	0.75	4	45
5–10	4 736	0.75	1.10	0.85	5	16
>10	76	0.76	1.14	0.78	7	10
TAO vs. NSCAT						
0–24	1 780	–0.26	0.92	0.92	5	20
0–5	515	–0.70	1.18	0.74	2	33
5–10	1 246	–0.08	0.79	0.83	7	11
>10	19	0.03	0.82	0.78	10	5

difference is consistent and the bias is about 1 m/s. This may be related to the south equatorial current effect on scatterometer backscatter coefficient measurements (Quilfen et al., 2001). Indeed, the buoy samples the absolute wind, whereas the scatterometer samples the relative wind. The highest discrepancy between the TAO and scatterometer winds (bias greater than 1.5 m/s) occurred between May and December 1998. During this period, several scatterometer-retrieved winds are not valid (especially during May and June 1998), and the TAO buoy moored at this location reported high variable wind speeds of about 7 m/s, exceeding climatology by 1 m/s. The

standard deviation of weekly averaged buoy wind speed varies between 0.90 and 1.90 m/s (72% of standard deviation values are great than 1.20 m/s). Furthermore, the analysis of oceanic current measured at 2°N and 110°W indicates that its magnitude was about 50 cm/s from May through December 1998, and for the same months during the period 1992–1997 the average current magnitude was 30 cm/s. The comparisons between the NDBC and scatterometer-averaged wind speed time series do not exhibit any systematic bias (an example is shown in **Figure 8a**). At some locations a seasonal variation in behavior is found. The bias tends to be positive in winter and

Table 4. Comparison of averaged weekly wind speed and direction estimated from the ODAS buoy measurements and from the ERS-2 and NSCAT scatterometer observations.

Buoy wind speed range (m/s)	Length	Wind speed			Wind direction	
		Bias (m/s)	RMS (m/s)	ρ	Bias ($^{\circ}$)	SD ($^{\circ}$)
ODAS vs. ERS-2						
0–24	222	–0.73	1.69	0.84	1	38
0–5	10	–1.26	2.01	0.72	31	75
5–10	155	–0.61	1.68	0.80	3	39
>10	57	–0.83	1.50	0.80	4	22
ODAS vs. NSCAT						
0–24	194	–0.65	1.52	0.89	2	30
0–5	6	–1.29	2.07	0.72	14	76
5–10	118	–0.62	1.44	0.81	1	30
>10	70	–0.57	1.47	0.86	9	22

**Figure 7.** Scatterplot of weekly analyzed scatterometer wind speeds calculated from the ERS-1, ERS-2, and NSCAT versus weekly averaged buoy wind speeds estimated from the NDBC, TAO, and ODAS. *a*, intercept on the *y* axis; *b*, slope of the regression line.

negative in summer. This may be related to the dependence of wind speed residuals on buoy wind speed ranges illustrated by the results of **Table 2**. For the ODAS (not shown), scatterometer-averaged wind speeds are consistently higher than buoy estimates. The bias tends to be large between October and December 1996, however, when the correlation coefficient is about 0.69, 22% lower than that for the whole

period. Some discrepancies between buoys and scatterometers are related to the sampling errors of scatterometer wind fields (Equation (3)). For instance, between July and August 1996, the ERS-2 error exceeds 2 m/s due to the relatively small number of scatterometer observations available to estimate the gridded fields.

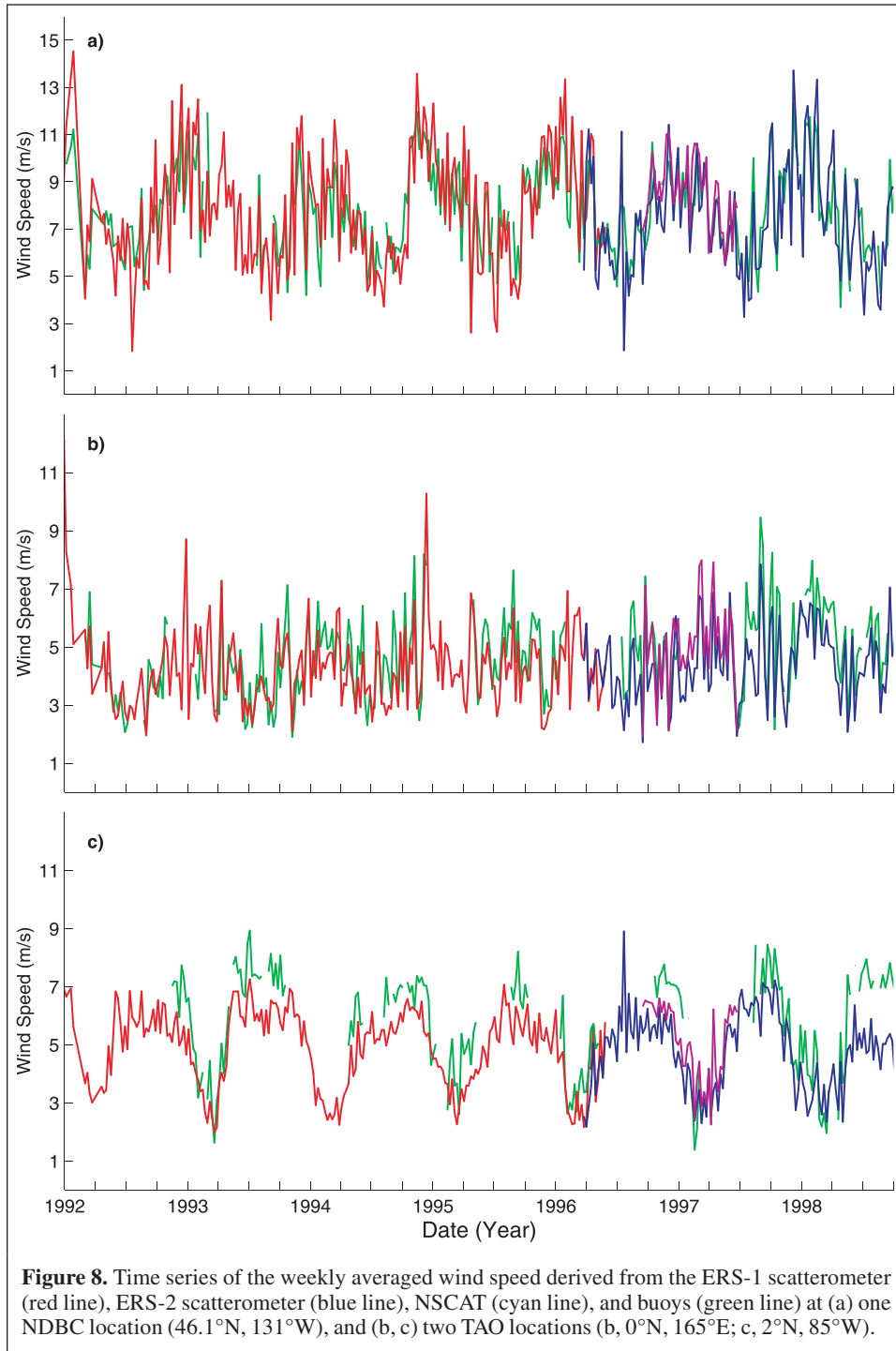


Figure 8. Time series of the weekly averaged wind speed derived from the ERS-1 scatterometer (red line), ERS-2 scatterometer (blue line), NSCAT (cyan line), and buoys (green line) at (a) one NDBC location (46.1°N, 131°W), and (b, c) two TAO locations (b, 0°N, 165°E; c, 2°N, 85°W).

Lastly, the dependence of the residuals on the buoy latitude is investigated. More than 80% of the latitudinal differences are less than 0.50 m/s. Between latitudes 8°S and 2°N (TAO array), the bias (buoy minus scatterometer) is positive and continues with increasing latitude. This dependency is consistent with the results shown earlier and may be due to current and sea state. From 5°N to 45°N, the bias decreases slightly. At high latitudes, where the wind is highly variable, scatterometer weekly wind speeds tend to be overestimated compared with buoy estimates. This is mainly related to the methods used to

estimate average wind data from scatterometers and buoys and the sampling scheme. The analysis of the RMS behavior according to latitudes confirms the latter result. Indeed, most of the RMS values of the difference between buoys and scatterometers are below 1.2 m/s, except at latitudes above 45°N.

To examine the agreement between average weekly scatterometer and buoy winds as a function of buoy latitude, the correlation coefficients are calculated for each latitude. The correlation coefficients are greater than 0.80 for all latitudes

and the difference between them is not significant at the 95% confidence level.

Scatterometer- and ECMWF-averaged wind comparisons

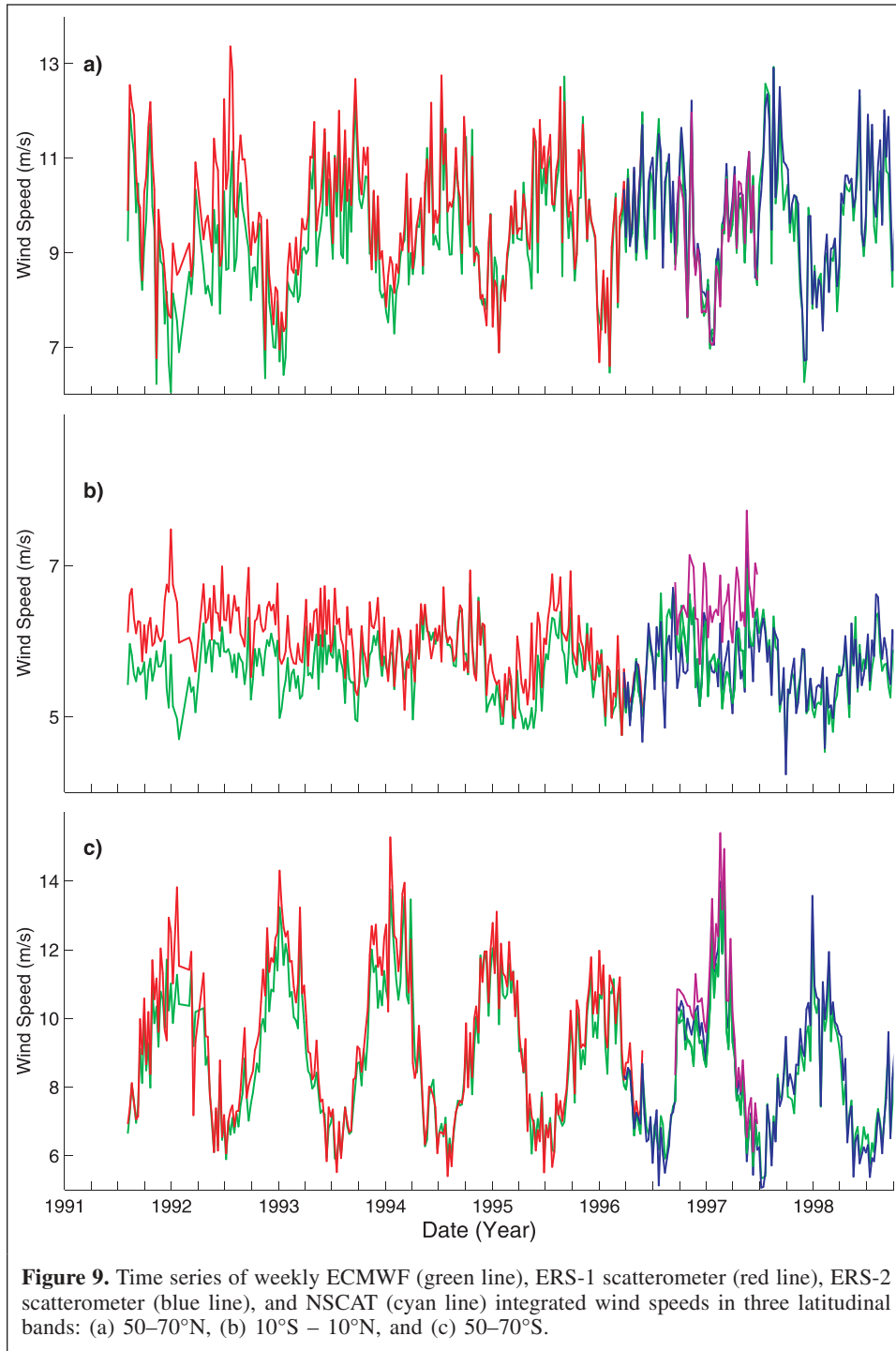
In this section, the new mean weekly and monthly scatterometer wind fields are compared with the ECMWF operational surface wind analysis (see the section Wind observations). Like several National Weather Prediction (NWP) systems, the ECMWF is a very complex analysis system, and forecasts are continually being improved. The ECMWF assimilates measurements from a variety of sources: satellites, buoys, and ships. It is important to note that ECMWF products are not used as “ground truth” surface winds. However, they involve the main known wind features at various scales and oceanic basins. Their use allows the investigation of scatterometer wind field patterns over a given oceanic basin and (or) time period. Furthermore, as the scatterometer data are uniformly processed, they can be used to evaluate the impact of the numerous changes occurring in the ECMWF forecast-analysis system. The mean weekly and monthly ECMWF wind speed, zonal component, and meridional component are computed from the 6 h global analysis datasets on $1.125 \times 1.125^\circ$ grid. The scatterometer sea ice mask is used to avoid ice.

The comparisons are performed over the global oceans for December and June for all ERS-1, ERS-2, and NSCAT periods. Only the ECMWF wind speeds above 3 m/s and estimated over oceanic regions are used. The statistics for the comparisons are summarized in **Table 5**. The correlations of wind speeds, zonal components, meridional components, and wind directions are high and exceed 0.89. For wind direction, the biases are small, and the RMS values are about 28° for ERS-1, 26° for ERS-2, and 17° for NSCAT. Even if the wind speed biases are rather low, the ERS-1 and NSCAT are biased high compared with the ECMWF by about 0.50 m/s, and the corresponding RMS values are 1.40 m/s for the ERS-1 and 1.03 m/s for the NSCAT. The number of high wind condition events derived from the ERS-1 and NSCAT is high with respect to the ECMWF. More than 6.5% of the ERS-1 and NSCAT wind speed estimates exceed 15 m/s. This percentage drops to 4.5% for the ECMWF. Comparisons between the ECMWF and the ERS-2 provide the

lowest bias and RMS values: 0.04 and 0.96 m/s, respectively. Most of the significant discrepancies between the ECMWF and scatterometers are located at high latitudes (60°S and 60°N). However, some cases of low correlations are found in middle latitudes. For instance, the correlation coefficient calculated in the south Atlantic region between 35°S and 45°S for the period 7–13 December 1992 is 0.42. For the aforementioned week and region, the kriging error (Equation (3)), measuring the quality of weekly averaged winds, does not exceed 1 m/s. The annual mean profiles, estimated as the longitudinal averages of the scatterometer and ECMWF winds in 1° of latitude, indicate that scatterometer and ECMWF wind features are very close. The highest wind values are found within the bands $50\text{--}60^\circ\text{S}$ and $50\text{--}60^\circ\text{N}$. The lowest winds occur within the equatorial regions. For instance, at 53°S , scatterometer and ECMWF provide annual wind speeds of about 9.5 m/s, whereas at 0° the annual wind speed is about 5 m/s. The highest differences exceeding 0.50 m/s are found in the band $55\text{--}65^\circ\text{N}$. However, such a calculation indicates that scatterometer wind speeds are greater than the ECMWF estimates almost everywhere. **Figure 9** displays examples of latitudinal scatterometer and ECMWF weekly wind speed comparisons. The time series are calculated from $1 \times 1^\circ$ grid points integrated over three 20° of latitude bands over the Atlantic Ocean and show that the correlation is high and roughly constant over the whole period. The scatterometer and ECMWF winds exhibit similar features. In particular, the examples do not show any disturbing oscillations in scatterometer winds (Large, 1998). Furthermore, such calculations confirm that the ERS-1 scatterometer records higher winds than the ECMWF. The maximum differences between the ERS-1 and ECMWF winds occurred between 9 December 1991 and 24 February 1992, corresponding to many missing scatterometer observations due to the ERS-1 scatterometer calibration-validation process. However, the calculation of the relative difference $((W_{\text{ECMWF}} - W_{\text{SCAT}}) / (W_{\text{ECMWF}} + W_{\text{SCAT}}) / 2$, where W_{SCAT} is the scatterometer wind speed at a height of 10 m) indicates that, on average, their values in equatorial regions decreased from 12% to 2% between March 1992 and September 1994, whereas in high-latitude regions these values are nearly steady at about 5%. For the ERS-2, the differences between the ECMWF and scatterometer winds are the lowest. The ERS-2 scatterometer measurements have been assimilated with the ECMWF since April 1996. Except in the southern Atlantic Ocean, average weekly winds estimated from the NSCAT observations are higher than the ECMWF wind estimates. The variability of the difference between the ECMWF and scatterometer weekly wind fields is investigated in terms of RMS difference (not shown in the figures). Excluding periods when large numbers of scatterometer observations are missing, the average RMS difference in wind speed is less than 1.50 m/s in the middle and tropical latitudes. In high latitudes and due to high wind variability, the RMS difference values are high and about 2 m/s. Similar geographical features are found in terms of wind components. As expected, the RMS difference between the ECMWF and ERS-2 is 0.50 m/s lower than that between the

Table 5. Comparison of averaged weekly wind speed and wind direction estimated from the ECMWF wind analysis and from the ERS-1, ERS-2, and NSCAT scatterometer observations.

Wind speed			Wind direction	
Bias (m/s)	RMS (m/s)	ρ	Bias ($^\circ$)	SD ($^\circ$)
ECMWF vs. ERS-1				
-0.39	1.42	0.89	1	28
ECMWF vs. ERS-2				
0.04	0.96	0.94	0	26
ECMWF vs. NSCAT				
-0.57	1.03	0.92	5	17

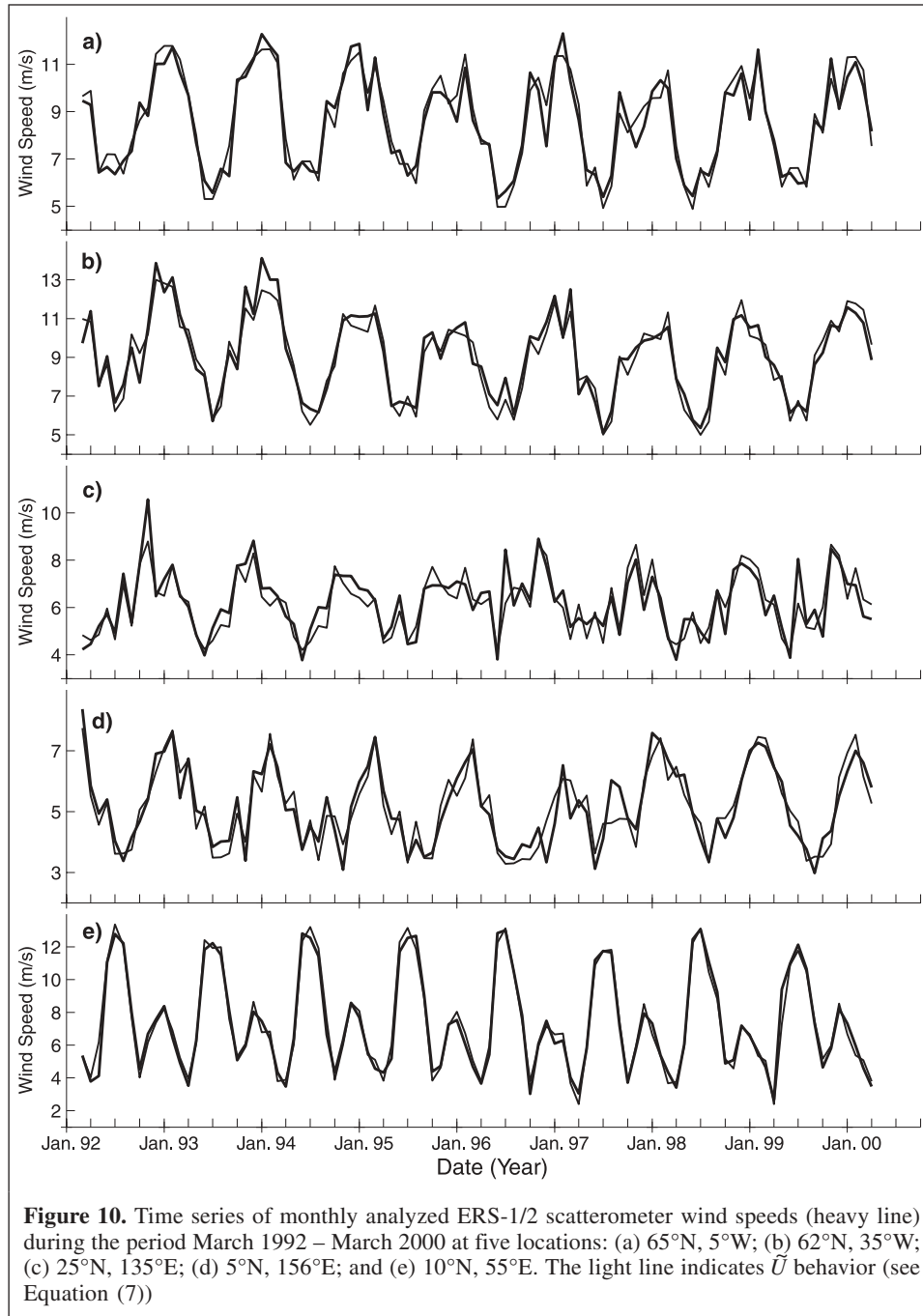


ECMWF and ERS-1. The analysis of the RMS difference patterns with time indicates that there is a decreasing trend mainly related to the ECMWF model changes (ECMWF, 1993). Furthermore, the RMS features are highly correlated with seasonal wind variability. For instance, in high northern latitudes the RMS differences are lower between April and September, with a mean value of about 0.80 m/s for wind speed. The behavior of the RMS differences between the ECMWF and NSCAT weekly wind speed and components is

quite comparable to that estimated from the ECMWF and ERS-2 differences.

Wind field features

In this section the reliability of scatterometer gridded wind fields is investigated in terms of surface wind speed patterns, and particularly via mean wind climatology and seasonal and spatial variability. Indeed, several authors have investigated such surface wind patterns using a variety of data sources (see,



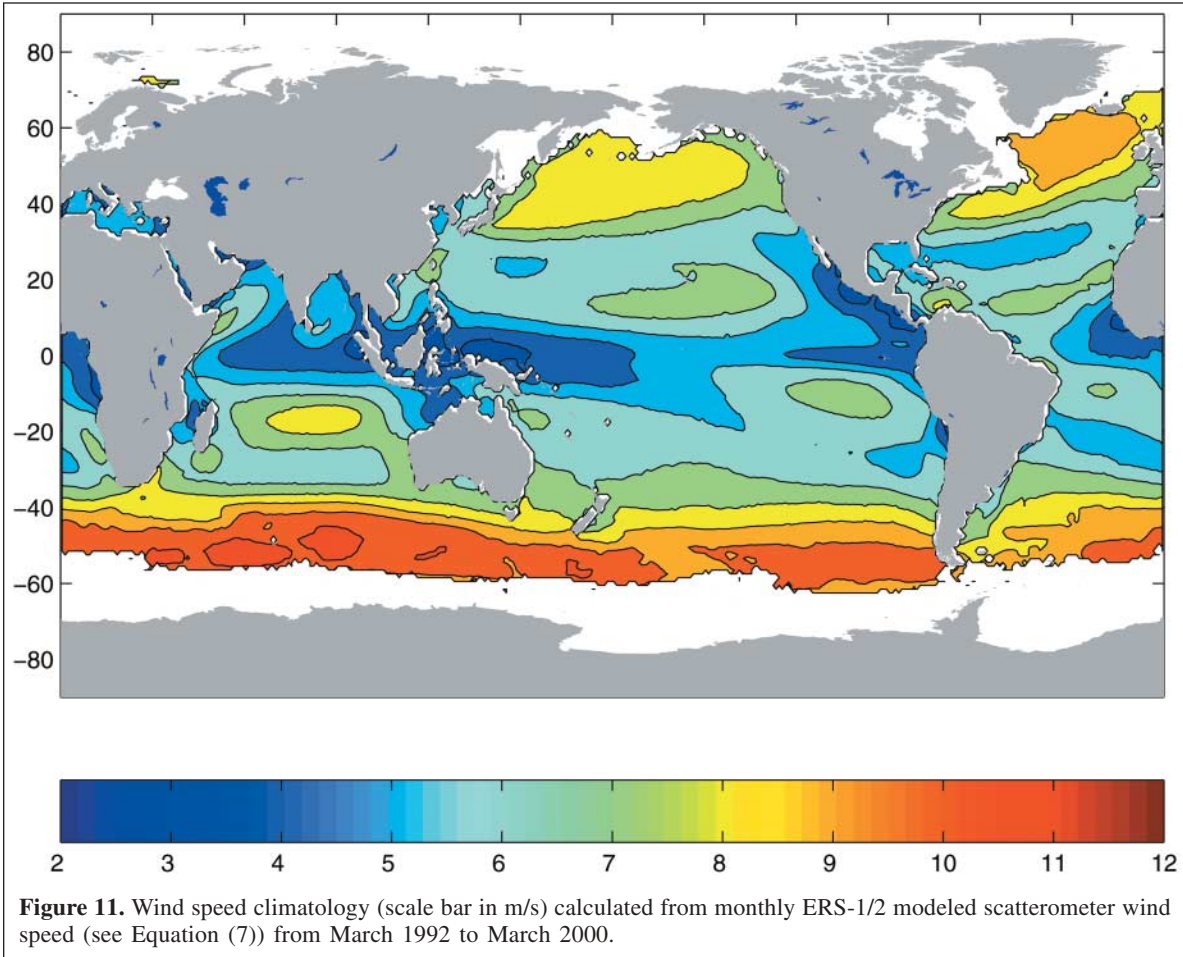
for instance, Hellerman and Rosenstein, 1983; Legler and O'Brien, 1988; Cardone et al., 1990; Trenberth, 1992; Gulev and Hasse, 1998). The aim of the present study is to match the previous climatological surface wind results. The wind speed analyses are performed with scatterometer monthly averaged wind fields, calculated from the ERS-1 and ERS-2 for the period March 1992 to March 2000. Over this 9 year period, the estimated signal frequency is from interseasonal to interannual.

The technique for long period data processing suggested by Lappo et al. (1986) is used to estimate the spatial features of the climatological means and the seasonal to annual variability.

Thus the following model for climatic wind speed time series is used:

$$\hat{U}(t) = \phi(t) + g(t) \quad (7)$$

where \tilde{U} is the mean monthly scatterometer wind speed, ϕ is a circular function fitting the multi-harmonical seasonal oscillations of surface wind speed:



$$\phi(t) = \sum_{i=1}^{i=2,4} \left[\alpha_i \cos\left(\frac{2\pi it}{T}\right) + \beta_i \sin\left(\frac{2\pi it}{T}\right) \right] \quad (8)$$

g is a polynomial function fitting the long-term year-to-year changes in scatterometer monthly wind speed:

$$g(t) = \sum_{i=0}^n a_i t^i \quad (9)$$

$T = 12$, and t is the time and varies from 1 to 98 (month number from March 1992 to March 2000). The summation index i in Equation (8) has values 1, 2, and 4. In Equation (9), $n = 2$. At each grip point, the coefficients α_i , β_i , and a_i are determined as the minimum of the function F measuring the difference between wind speed model (Equation (7)) and monthly wind speed estimates:

$$F = \sum_{i=1}^{98} \left[\frac{U(t) - \tilde{U}(t)}{\sigma_U(t)} \right]^2 \quad (10)$$

where σ_U is the kriging error associated with U (Equation (3)). Several parameters characterizing the wind variability can be estimated from harmonical-polynomial model (Equation (7)).

For instance, at the grid point the climatological mean is a_0 (Equation (9)) and the wind annual variability is $\sqrt{a_1^2 + \beta_1^2}$ (Equation (7)).

Figure 10 shows an example of comparisons between wind speed time series U and \tilde{U} at two locations in the Atlantic Ocean (65°N, 5°W; 62°N, 35°W), two locations in the Pacific Ocean (25°N, 135°E; 4°N, 165°E), and one location in the Indian Ocean (10°N, 55°E). The agreement between both wind speed estimates is good. The correlation coefficients between U and \tilde{U} are from 0.90 (**Figure 10c**) to 0.98 (**Figure 10d**). The main surface wind speed features estimated from scatterometer monthly wind fields are clearly revealed by \tilde{U} . For instance, both wind speed estimates indicate that the interannual variability of wind speed is characterized by a significant positive trend between March 1992 and 1995 (Diaz et al., 1995; Gulev, 1999). The trend is estimated through a linear model and is significant based on Student's t test (Gulev, 1999). Since 1996, the interannual variability exhibits a negative trend. At one of the locations in the Atlantic Ocean (62°N, 35°W), U and \tilde{U} wind speed variabilities indicate a significant negative trend in December and January of about -0.20 m/s. **Figure 10d** indicates that both wind estimates provide maximum and minimum values of surface winds in March and October, respectively. The wind anomaly related to the El Niño event

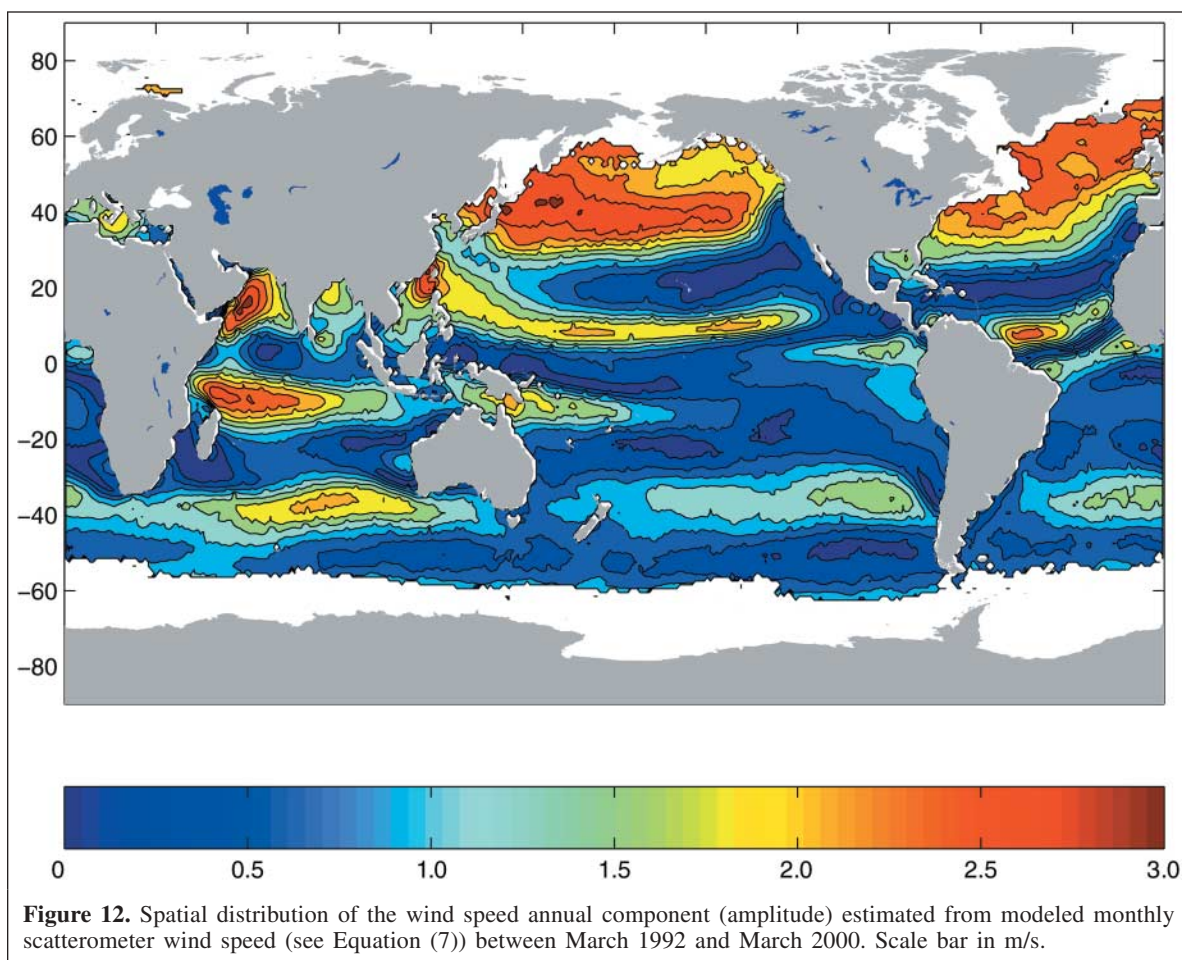


Figure 12. Spatial distribution of the wind speed annual component (amplitude) estimated from modeled monthly scatterometer wind speed (see Equation (7)) between March 1992 and March 2000. Scale bar in m/s.

during 1997–1998 is clearly depicted. The correlation between U and \tilde{U} in the Indian Ocean is high (**Figure 10e**). This is mainly due to the highly consistent nature of the Indian monsoon system. Measured and modeled monthly wind speeds reveal two peaks, the first in June and the second in December. During 1997, wind speed values are low with respect to the mean wind climatology of the region. This is related to the El Niño event (Yasunari, 1991).

The climatological mean monthly scatterometer wind speed \tilde{U} is shown in **Figure 11**. The major features known to exist in the wind speed field are clearly evident. Over most of northern latitudes located between 40°N and 60°N, the wind speed lies between 7 and 9 m/s. Its spatial patterns are oriented southwest to northeast. The highest wind speeds are found in the Southern Hemisphere between 40°S and 60°S. Their spatial patterns are parallel to the latitudes. A region of high wind speed is depicted in the southern Indian Ocean. As expected, the weakest climatological means of surface wind speed are found in tropical areas, particularly in the eastern and western parts of the Pacific Ocean and in the western part of the Atlantic Ocean. In both areas, the wind speed does not exceed 4 m/s. Medium wind speed ranges (6–7 m/s) characterize the trade winds regions. There are westerlies located on each side of the tropical Atlantic and Pacific oceans, particularly the Pacific.

The spatial pattern of the wind speed annual variability, estimated from Equation (7), is shown in **Figure 12**. The annual component accounts for about 87% of the total variability. As expected, the largest areas of high wind variability are located in the northern Atlantic and Pacific oceans (40–60°N). Two narrow latitudinal bands of high variability are depicted within the inter-tropical regions of the Atlantic and Pacific oceans. This is in connection with InterTropical Convergence Zone (ITCZ) variability. In the Indian Ocean, the highest variability is associated with monsoon events in the Arabian Sea. Other large areas of high annual variability are located in the southern Indian Ocean, the Bay of Bengal, the South China Sea, and northeast of Australia. The annual variability of surface wind speed is quite low in the high latitudes of the Southern Ocean hotbed of high wind speeds. In terms of semi-annual variability, only regions associated with the Asian monsoon system have high and significant values. The following regions can be classified according to the semi-annual features: Arabian Sea, Bay of Bengal, South China Sea, and north of Australian.

Summary

Ensuring the quality and consistency of long-term series of surface wind fields is a crucial task. The importance of this task is highlighted through the requirements of national and

international oceanic programs, such as MERCATOR, the French component of the Global Oceanography Data Assimilation Experiment (GODAE), and the Global Climate Observing System (GCOS).

In this paper we have provided background to the calculation of gridded wind fields from global scatterometer observations. The accuracy of these calculations was established through comparisons with averaged winds derived from buoys at various locations in the Pacific and Atlantic oceans. The bias between satellite and buoy weekly wind speed ranged between 0 and 0.80 m/s, and the corresponding standard deviation ranged between 0.80 and 1.6 m/s. The main discrepancies are related to scatterometer sampling errors, which may be improved when merging satellite observations from several satellites.

In an examination of the global features of the scatterometer wind fields, the ECMWF wind vector analyses were used. The comparisons revealed that both sources provide highly correlated surface winds. The RMS differences for wind speed and direction are less than 2 m/s and 20°, respectively. On average, the ERS-1 and NSCAT provide higher winds than the ECMWF. The wind fields calculated from the ERS-2 scatterometer observations exhibit the best correlation with those from the ECMWF. This result may be related to the assimilation of ERS-2 winds into the ECMWF analysis system. The comparison between scatterometer and ECMWF times indicated that in the tropical region (10°S–10°N) the difference between the ECMWF and scatterometer weekly mean winds was significant between 1992 and 1994, and became small with time.

The high correlation between satellite and buoy winds suggests that remotely sensed winds should be used in combination with in situ measurements and models to improve our understanding of the interactions between the atmosphere and the ocean.

The weekly and monthly surface wind fields, calculated from scatterometer measurements, are part of World Ocean Circulation Experiment (WOCE) data sets, and are also available from the Centre ERS d'Archivage et de Traitement (CERSAT/IFREMER) (available at: <<http://www.ifremer.fr:80/cersat>>).

References

- Andrews, P.L., and Bell, R.S. 1998. Optimizing the United Kingdom Meteorological Office data assimilation for ERS-1 scatterometer winds. *Monthly Weather Review*, Vol. 126, pp. 736–746.
- Atlas, R. 1997. Atmospheric observations and experiments to assess their usefulness in data assimilation. *Journal of the Meteorological Society of Japan*, Vol. 75, pp. 111–130.
- Barnier, B., Cappella, J., and O'Brien, J.J. 1994. The use of satellite scatterometer winds to derive a primitive equation model in the Indian Ocean: the impact of the band-like sampling. *Journal of Geophysical Research*, Vol. 99, No. C7, pp. 14 187 – 14 196.
- Bentamy, A., Quilfen, Y., Queffeuou, P., and Cavanie, A. 1994. Calibration of the ERS-1 scatterometer C-band model. IFREMER Technical Report DRO/OS-94-01, IFREMER, Brest, France. 72pp.
- Bentamy, A., Quilfen, Y., Gohin, F., Grima, N., Lenaour, M., and Servain, J. 1996. Determination and validation of average wind fields from ERS-1 scatterometer measurements. *Global Atmosphere and Ocean System*, Vol. 4, pp. 1–29.
- Bentamy, A., Grima, N., and Quilfen, Y. 1998. Validation of the gridded weekly and monthly wind fields calculated from ERS-1 scatterometer wind observations. *Global Atmosphere and Ocean System*, Vol. 6, pp. 373–396.
- Cardone, V.J., Greenwood, J.G., and Cane, M.A. 1990. On trends in historical marine wind data. *Journal of Climate*, Vol. 3, pp. 113–127.
- Caruso, M., Dickinson, S., Kelly, K., Spillane, M., Mangum, L., McPhaden, M., and Stratton, L. 1999. Evaluation of NSCAT scatterometer winds using Equatorial Pacific buoy observations. Technical Report, Applied Physics Laboratory, University of Washington, Seattle, Wash. 60pp.
- CERSAT. 1998. Mean wind field products, user manual. Technical Report, IFREMER, Brest, France (available at: <http://www.ifremer.fr:80/cersat/ACTIVITE/ATLAS/DIFF/F_SOFTDO.HTM>). 57pp.
- Diaz, H.F., Quan, X., and Fu, C. 1995. Marine surface wind changes during 1978–1992: an estimation based on COADS. In *Proceedings of the International COADS Winds Workshop*, Kiel, Germany. National Oceanic and Atmospheric Administration (NOAA), Washington, D.C. pp. 48–67.
- Ebutchi, N., and Wada, T. 2001. Construction of wind stress fields using optimum interpolation with self-determined autocorrelation function. In *Proceedings of the WCRP/SCOR*, May 21–24, Washington, D.C. (available at: <<http://www.soc.soton.ac.uk/JRD/MET/WGASF/workshop>>).
- ECMWF. 1993. The description of the ECMWF/WCRP level III-A atmospheric data archive. Technical Attachment, European Centre for Medium-Range Weather Forecasts (ECMWF) Report, Shinfield Park, Reading, U.K.
- ECMWF. 1995. User guide to ECMWF products 2.1. European Centre for Medium-Range Weather Forecasts (ECMWF), Shinfield Park, Reading, U.K. 71pp.
- Gilhousen, D.B. 1987. A field evaluation of NDBC moored buoy winds. *Journal of Atmospheric and Oceanic Technology*, Vol. 4, pp. 94–104.
- Graber, H.C., Ebutchi, N., and Vakkayil, R. 1996. Evaluation of ERS-1 scatterometer winds with wind and wave ocean buoy observations. Technical Report RSMAS 96-003, Division of Applied Marine Physics, RSMAS, University of Miami, Miami, Fla. 58pp.
- Graber, H.C., Bentamy, A., and Ebutchi, N. 1997. Evaluation of NSCAT scatterometer winds with ocean buoy observations. In *Proceedings of the NASA Scatterometer Science Symposium*, 10–14 Nov. 1997, Maui, Hawaii. pp. 106–107.
- Grima, N., Bentamy, A., Katsaros, K., Quilfen, Y., Delecluse, P., and Levy, C. 1999. Sensitivity of an oceanic general circulation model forced by satellite wind stress fields. *Journal of Geophysical Research*, Vol. 104, No. C4, pp. 7967–7989.
- Gulev, S.K. 1999. Comparison of COADS Release 1a winds with instrumental measurements in the northwest Atlantic. *Journal of Atmospheric and Oceanic Technology*, Vol. 10, pp. 133–145.
- Gulev, S.K., and Hasse, L. 1998. North Atlantic wind waves and wind stress fields from voluntary observing ship data. *Journal of Physical Oceanography*, Vol. 28, pp. 1107–1130.

- Hayes, S.P., Mangum, L.J., Picaud, J., Takeuchi, K., and TOGA-TAO. 1991. A moored array for real-time measurements in the tropical Pacific Ocean. *Bulletin of the American Meteorological Society*, Vol. 72, pp. 339–347.
- Hellerman, S., and Rosenstein, M. 1983. Normal monthly wind stress over the open ocean with error estimates. *Journal of Physical Oceanography*, Vol. 13, pp. 1093–1105.
- Jet Propulsion Laboratory. 1998. NASA scatterometer science data product user's manual; overview & geophysical data products version 1.2. JPL D-12985, Jet Propulsion Laboratory, California Institute of Technology, Pasadena, Calif. 66pp.
- Lappo, S.S., Beleav, K.P., Muzychenko, A.G., and Selemenov, K.M. 1986. Statistical analysis of multiyear SST series in the North Atlantic and the North Pacific. In *Hydrometeorological features of mid-latitude oceans*. Gidrometeoizdat, Moscow, pp. 10–22.
- Large, W.G. 1998. WOCE ocean surface boundary conditions. In *Proceedings of World Ocean Circulation Experiment WOCE SSG*, Brest, France. pp. 16–22.
- Legler, D.M., and O'Brien, J.J. 1988. Tropical Pacific wind stress analysis for TOGA. Technical Series Ioc., Vol. 33, pp. 11–17
- Liu, W., Katsaros, K., and Businger, J.A. 1979. Bulk parameterization of air-sea exchanges of heat and water vapor including the molecular constraints at the interface. *Journal of Atmospheric Sciences*, Vol. 36, pp. 1722–1735.
- Maroni, C. 1995. Offline wind field production. CERSAT News, Issue 5, IFREMER Publication, February 2–3 (available at: <<http://www.ifremer.fr:80/cersat/>>).
- Millif, R.F., Large, G.W., Holland, R.H., and McWilliams, J.C. 1996. The general circulation responses of high resolution North Atlantic ocean models to synthetic scatterometer winds. *Journal of Physical Oceanography*, Vol. 26, pp. 1747–1768.
- Quilfen, Y., Bentamy, A., Katsaros, K., and Lorand, G. 1999. Estimation of ocean-atmosphere turbulent fluxes from satellite measurements. In *OCEANOBS99, Proceedings of the International Conference on the Ocean Observing System for Climate*, St. Raphael, France, pp. 18–22.
- Quilfen, Y., Bentamy, A., Delecluse, P., Katsaros, K.B., and Grima, N. 2000. Prediction of sea level anomalies using ocean circulation model forced by scatterometer wind and validation using TOPEX/Poseidon data. *IEEE Transactions on Geoscience and Remote Sensing*, Vol. 38, No. 4, pp. 1871–1884.
- Quilfen, Y., Chapron, B., and Vandemark, D. 2001. On the ERS scatterometer wind measurement accuracy: evidence of seasonal and regional biases. *Journal of Atmospheric and Oceanic Technology*, Vol. 18, pp. 1684–1697.
- Stoffelen, A., and Anderson, D. 1997. Ambiguity removal and assimilation of scatterometer data. *Quarterly Journal of the Royal Meteorological Society*, Vol. 123, pp. 491–518.
- Trenberth, K.E. 1992. Global analyses from ECMWF and atlas of 1000 to 10mb circulation statistics. Technical Note NCAR/TN-317 + STR, National Centre for Atmospheric Research, Boulder, Colo. 191pp.
- Yasunari, T. 1991. The monsoon year — a new concept of the climatic year in the tropics. *Bulletin of the American Meteorological Society*, Vol. 72, pp. 1331–1338.